Improved laser glass cutting by spatio-temporal control of energy deposition using bursts of femtosecond pulses

K. Mishchik, R. Beuton, O. Dematteo Caulier, Stefan Skupin, B. Chimier, G. Duchateau, B. Chassagne, R. Kling, C. Honninger, E. Mottay, et al.

Research Article | Vol. 25, No. 26 | 25 Dec 2017 | OPTICS EXPRESS 33271
Optics EXPRESS

Improved laser glass cutting by spatio-temporal control of energy deposition using bursts of femtosecond pulses

K. Mishchik,[1,2,*] R. Beuton,[2] O. Dematteo Caulier,[2] S. Skupin,[2,3] B. Chimier,[2] G. Duchateau,[2] B. Chassagne,[4] R. Kling,[4] C. Hönninger,[1] E. Mottay,[1] and J. Lopez[2]

[1]*Amplitude Systèmes, 11 avenue de Canteranne, 33600 Pessac, France*
[2]*Université Bordeaux CNRS CEA, CELIA UMR5107, 33405 Talence, France*
[3]*Institut Lumière Matière, UMR 5306 Université Lyon 1 - CNRS, Université de Lyon, 69622 Villeurbanne, France*
[4]*ALPhANOV, Rue François Mitterrand, 33400 Talence, France*
[*]*konstantin.mishchik@amplitude-laser.com*

Abstract: We demonstrate the advantage of combining non-diffractive beam shapes and femtosecond bursts for volume laser processing of transparent materials. By re-distribution of the single laser pulse energy into several sub-pulses with 25 ns time delay, the energy deposition in the material can be enhanced significantly. Our combined experimental and theoretical analysis shows that in burst-mode detrimental defocusing by the laser generated plasma is reduced, and the non-diffractive beam shape prevails. At the same time, heat accumulation during the interaction with the burst leads to temperatures high enough to induce material melting and even in-volume cracks. In an exemplary case study, we demonstrate that the formation of these cracks can be controlled to allow high-speed and high-quality glass cutting.

OCIS codes: (140.3390) Laser materials processing; (320.2250) Femtosecond phenomena; (160.2750) Glass and other amorphous materials.

References and links

1. J.-S. Park, H. Chae, H. K. Chung, and S. I. Lee, "Thin film encapsulation for flexible AM-OLED: a review," Semicond. Sci. Tech. **26**, 34001 (2011).
2. S. Garner, S. Glaesemann, and X. Li, "Ultra-slim flexible glass for roll-to-roll electronic device fabrication," Appl. Phys. A **116**, 403–407 (2014).
3. J. Deubener, G. Helsch, A. Moiseev, and H. Bornhöft, "Glasses for solar energy conversion systems," J. Eur. Ceram. Soc. **29**, 1203–1210 (2009).
4. R. R. Gattass and E. Mazur, "Femtosecond laser micromachining in transparent materials," Nat. Photonics **2**, 219–225 (2008).
5. S. A. Hosseini and P. R. Herman, "Method of material processing by laser filamentation," (2016). US Patent 9,296,066.
6. M. Kumkar, L. Bauer, S. Russ, M. Wendel, J. Kleiner, D. Grossmann, K. Bergner, and S. Nolte, "Comparison of different processes for separation of glass and crystals using ultrashort pulsed lasers," Proc. SPIE **8972**, 897214 (2014).
7. M. K. Bhuyan, O. Jedrkiewicz, V. Sabonis, M. Mikutis, S. Recchia, A. Aprea, M. Bollani, and P. Di Trapani, "High-speed laser-assisted cutting of strong transparent materials using picosecond Bessel beams," Appl. Phys. A **120**, 443–446 (2015).
8. A. R. Collins and G. M. O'Connor, "Mechanically inspired laser scribing of thin flexible glass," Opt. Lett. **40**, 4811–4814 (2015).
9. F. Hendricks, V. V. Matylitsky, M. Domke, and H. Huber, "Time-resolved study of femtosecond laser induced micro-modifications inside transparent brittle materials," Proc. of SPIE **9740**, 97401A (2016).
10. K. Mishchik, B. Chassagne, C. Javaux-Léger, C. Hönninger, E. Mottay, R. Kling, and J. Lopez, "Dash line glass-and sapphire-cutting with high power USP laser," Proc. SPIE **9740**, 97400W (2016).
11. L. Rapp, R. Meyer, L. Furfaro, C. Billet, R. Giust, and F. Courvoisier, "High speed cleaving of crystals with ultrafast Bessel beams," Opt. Express **25**, 9312–9317 (2017).
12. R. Herman and T. Wiggins, "Production and uses of diffractionless beams," J. Opt. Soc. Am. A **8**, 932–942 (1991).

#308614 https://doi.org/10.1364/OE.25.033271
Journal © 2017 Received 6 Oct 2017; revised 15 Nov 2017; accepted 24 Nov 2017; published 21 Dec 2017

Optics EXPRESS

13. P. Polesana, M. Franco, A. Couairon, D. Faccio, and P. Di Trapani, "Filamentation in Kerr media from pulsed Bessel beams," Phys. Rev. A **77**, 043814 (2008).
14. D. Faccio, E. Rubino, A. Lotti, A. Couairon, A. Dubietis, G. Tamošauskas, D. G. Papazoglou, and S. Tzortzakis, "Nonlinear light-matter interaction with femtosecond high-angle Bessel beams," Phys. Rev. A **85**, 33829 (2012).
15. A. Couairon and A. Mysyrowicz, "Femtosecond filamentation in transparent media," Phys. Rep. **441**, 47–189 (2007).
16. P. K. Velpula, M. K. Bhuyan, F. Courvoisier, H. Zhang, J.-P. Colombier, and R. Stoian, "Spatio-temporal dynamics in nondiffractive Bessel ultrafast laser nanoscale volume structuring," Laser Photonics Rev. **244**, 230–244 (2016).
17. V. Garzillo, V. Jukna, A. Couairon, R. Grigutis, P. Di Trapani, and O. Jedrkiewicz, "Optimization of laser energy deposition for single-shot high aspect-ratio microstructuring of thick BK7 glass," J. Appl. Phys. **120**, 13102 (2016).
18. M. K. Bhuyan, F. Courvoisier, P.-A. Lacourt, M. Jacquot, L. Furfaro, M. J. Withford, and J. M. Dudley, "High aspect ratio taper-free microchannel fabrication using femtosecond Bessel beams." Opt. Express **18**, 566–574 (2010).
19. M. Clerici, D. Faccio, E. Rubino, A. Lotti, A. Couairon, and P. Di Trapani, "Space–time focusing of Bessel-like pulses," Opt. Lett. **35**, 3267–3269 (2010).
20. R. Kammel, R. Ackermann, J. Thomas, J. Götte, S. Skupin, A. Tünnermann, and S. Nolte, "Enhancing precision in fs-laser material processing by simultaneous spatial and temporal focusing," Light Sci. Appl. **3**, e169 (2014).
21. A. Marcinkevcius, S. Juodkazis, S. Matsuo, V. Mizeikis, and H. Misawa, "Application of Bessel Beams for Microfabrication of Dielectrics by Femtosecond Laser," Jpn. J. Appl. Phys. **40**, 1197–1199 (2001).
22. J. Amako, D. Sawaki, and E. Fujii, "Microstructuring transparent materials by use of nondiffracting ultrashort pulse beams generated by diffractive optics," J. Opt. Soc. Am. B **20**, 2562–2568 (2003).
23. D. Grojo, A. Mouskeftaras, P. Delaporte, and S. Lei, "Limitations to laser machining of silicon using femtosecond micro-Bessel beams in the infrared," J. Appl. Phys. **117**, 153105 (2015).
24. F. He, J. Yu, Y. Tan, W. Chu, C. Zhou, Y. Cheng, and K. Sugioka, "Tailoring femtosecond 1.5-μm Bessel beams for manufacturing high-aspect-ratio through-silicon vias," Sci. Rep. **7**, 40785 (2017).
25. N. P. Bansal and R. H. Doremus, *Handbook of glass properties* (Elsevier, 2013).
26. "EAGLE XG® Slim. Product Information Sheet," https://www.corning.com.
27. "D263® T eco Thin Glass. Product Information," http://www.schott.com.
28. A. Rosenfeld, M. Lorenz, R. Stoian, and D. Ashkenasi, "Ultrashort-laser-pulse damage threshold of transparent materials and the role of incubation," Appl. Phys. A **69**, S373–S376 (1999).
29. S. M. Eaton, H. Zhang, P. R. Herman, F. Yoshino, L. Shah, J. Bovatsek, and A. Y. Arai, "Heat accumulation effects in femtosecond laser-written waveguides with variable repetition rate," Opt. Express **13**, 4708–4716 (2005).
30. J. B. Lonzaga, S. M. Avanesyan, S. C. Langford, and J. T. Dickinson, "Color center formation in soda-lime glass with femtosecond laser pulses," J. Appl. Phys. **94**, 4332–4340 (2003).
31. A. M. Streltsov and N. F. Borrelli, "Study of femtosecond-laser-written waveguides in glasses," J. Opt. Soc. Am. B **19**, 2496–2504 (2002).
32. O. Brzobohaty, T. Cizmar, and P. Zemanek, "High quality quasi-Bessel beam generated by round-tip axicon," Opt. Express **16**, 12688–12700 (2008).
33. J. Dudutis, P. Gecys, and G. Raciukaitis, "Non-ideal axicon-generated Bessel beam application for intra-volume glass modification," Opt. Express **24**, 28433–28443 (2016).
34. O. Dematteo Caulier, K. Mishchik, B. Chimier, S. Skupin, A. Bourgeade, C. Javaux Léger, R. Kling, C. Hönninger, J. Lopez, V. Tikhonchuk, and Others, "Femtosecond laser pulse train interaction with dielectric materials," App. Phys. Lett. **107**, 181110 (2015).
35. L. Bergé, S. Skupin, R. Nuter, J. Kasparian, and J.-P. Wolf, "Ultrashort filaments of light in weakly ionized, optically transparent media," Reports Prog. Phys. **70**, 1633 (2007).
36. M. Kolesik and J. V. Moloney, "Nonlinear optical pulse propagation simulation: From Maxwell's to unidirectional equations," Phys. Rev. E **70**, 36604 (2004).
37. L. V. Keldysh, "Ionization in the field of a strong electromagnetic wave," Sov. Phys. JETP **20**, 1307–1314 (1965).
38. S. S. Mao, F. Quéré, S. Guizard, X. Mao, R. E. Russo, G. Petite, and P. Martin, "Dynamics of femtosecond laser interactions with dielectrics," Appl. Phys. A **79**, 1695–1709 (2004).
39. K. Saito and A. J. Ikushima, "Absorption edge in silica glass," Phys. Rev. B **62**, 8584 (2000).
40. A. A. Griffith, "The phenomena of rupture and flow in solids," Phil. Trans. R. Soc. London A **221**, 163–198 (1921).
41. R. B. Hetnarski, M. R. Eslami, and G. M. L. Gladwell, *Thermal stresses: advanced theory and applications*, vol. 158 (Springer, 2009).
42. R. E. Mould, "The strength of inorganic glasses," in "Fundamental Phenomena in the Materials Sciences, V. 4," (Springer, 1967), pp. 119–149.

1. Introduction

Glass and other ceramics are very important materials with a wide range of industrial applications. Just to mention few examples, these materials are indispensable for the fabrication of TFT and organic LED screens, touch sensors, medical devices, *etc.* [1–3]. Many of these applications require precise and accurate micro-machining, which remains challenging due to the brittleness

Optics EXPRESS

and unfavorable thermal properties of these materials. Recently, intense ultrashort laser pulses have emerged as an attractive tool for processing of glasses and other brittle dielectrics. Because laser energy absorption is highly nonlinear, the machining process can be controlled very precisely, and detrimental thermal effects are minimized [4]. Focused ultrashort laser pulses may induce highly localized structural modifications, and, if the deposited energy density is particularly high, laser-induced stresses and irreversible volume modifications allow non-ablative cutting [5–11].

Traditionally the regime of high energy deposition is achieved by use of an objective lens with high numerical aperture NA>0.4 [4], however the depth of the modified volume will be limited by the Rayleigh length, typically less than 20 μm. In glass cutting applications, a uniform energy deposition along the total material thickness is required, largely exceeding the focus depth of conventional Gaussian beams. This limitation can be overcome by using non-diffractive Bessel beams [12]. For example, a Bessel-Gaussian beam is produced by interferences of an incident Gaussian beam with itself at a conical angle θ_B [cf. Fig. 1(a)]. A Bessel beam appears as a long and narrow filament surrounded by circles of higher interference orders. The diameter of the central intensity peak is only a few microns, but its extension along the optical axis may exceed several hundred microns.

A crucial point when it comes to applications is that these non-diffractive beams have to keep their structure in the presence of the highly nonlinear propagation effects, so that energy is deposited along their whole length [13]. In order to produce extending Bessel beams, hundreds of microns long, conical angles of $10^\circ<\theta_B<20^\circ$ are employed. In contrast to high-angle Bessel beams, the laser pulse gets strongly perturbed and defocused by the nonlinear Kerr effects and induced plasma [14], that is similar to the femtosecond (fs) filamentary propagation using low NA conventional focusing optics [15]. As a consequence, a relatively low free electrons concentration and weaker material damage than expected from linear propagation dynamics is observed [16, 17]. When even smaller conical angles $\theta_B<10^\circ$ are employed, these nonlinear effects completely prevent the formation of permanent modifications [17]. One way to overcome this problem is to pre-chirp the laser pulse [16, 18] or use space-time focusing [19, 20] and rely on temporal compression dynamics to increase the laser intensity and, thus, the energy deposition inside the medium. By using such techniques, Bessel beams were successfully employed for microstructuring of glass and semiconductors [21–23], drilling of microchannels in glass and silicon [18, 24], as well as for cutting of thick glasses [7].

In this work, we propose an alternative route to spatio-temporal control and enhancement of the energy deposition using Bessel-Gaussian beams. In the first part of the paper we will describe our method and its experimental implementation and results. The method relies on processing of the material using so-called bursts of fs-pulses. One burst consists of a few sub-pulses which propagate at a delay of a few tens of nanoseconds (ns). Thus, instead of exposing the material to one pulse per inverse repetition rate, a short pulse train of sub-pulses hits the medium periodically, where the average power is the same. In the second part of the paper, we perform multi-scale numerical simulations fully supporting our experimental results. The simulation results indeed show that the sub-pulses in the burst undergo less perturbation during propagation because they produce less plasma. However, due to accumulation effects over the whole sub-pulse train the total energy deposition is enhanced. Finally, we demonstrate laser-cutting of glass samples with variable thickness and different thermo-mechanical properties with fs-bursts.

2. Experimental setup and results

An Yb-doped hybrid fiber/crystal laser system operating at 1030 nm (Yuja, Amplitude Systèmes, 10 W, 450 fs) is used as a source of ultrashort laser pulses. This system may operate in burst-mode, when few pulses from the oscillator are amplified in the hybrid fiber/crystal amplifier chain. The oscillator frequency of 40 MHz defines a separation of τ=25 ns between sub-pulses in the high-energy burst.

Optics EXPRESS

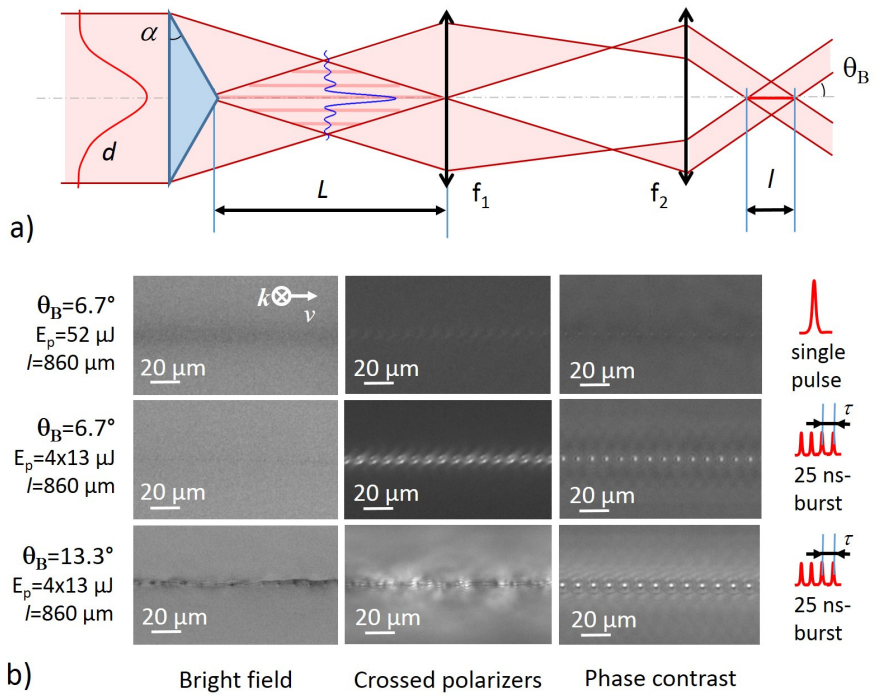

Fig. 1. a) Setup for the Bessel beam generation. The primary beam is produced with an axicon and projected to the focal region using a telescope setup with demagnification ratio $M=f_2/f_1$. b) Top-view micrographs of localized modification produced with 52 μJ Bessel beams in single-pulse mode (first row), or burst mode (second and third rows) were taken in transmission configuration using bright-field (left column), crossed-polarizers (center column), and phase-contrast illuminations (right column). In burst mode, four sub-pulses with 25 ns delay were employed. For all images, laser incidence was towards the plane of the figure, scanning was performed from left to right. The pulse duration was 450 fs (FWHM).

A sketch of the experimental setup is presented in Fig. 1(a). A primary zero-order Bessel beam is generated using an axicon and then projected inside the glass by means of a $4f$ afocal imaging system with a demagnification ratio of $M=f_2/f_1$. The incident Gaussian beam diameter is controlled by a variable beam expander (2×–10× by Jenoptik). The non-diffractive length of the Bessel beam can be adjusted by varying the beam diameter d, the base angle α of the axicon, and the demagnification M according to the relation $l = ndM^2/2\,(n_a - 1)\,\alpha$, where n_a is the refractive index of the axicon, and n is the refractive index of the processed glass. In this work, we have studied the nonlinear propagation of Bessel beams constructed at different cone angles $\theta_B = (n_a - 1)\,\alpha/Mn$. At the same time, we have preserved the length of the Bessel beam by adjusting the incident beam diameter d accordingly.

Three types of commercially available technical glasses were used in our experiment: soda-lime silicate glass [25], Eagle XG by Corning [26], and D263T glass by SCHOTT [27]. Soda-lime glass is available in the form of microscopic slides of 1mm thickness. Eagle and D263T glasses come as sheets with thickness <500 μm. All glasses have an excellent optical surface quality, so experiments could be performed after cleaning the samples with acetone. The relatively thick samples of soda-lime glass are suitable for investigating bulk processing at a wide range of focusing parameters. Therefore, all proof-of-concept experiments and numerical simulations were performed in soda-lime glass.

Optics EXPRESS

We compared in-volume modifications of soda-lime glass obtained with a 52 µJ single pulse and a 52 µJ burst (on the target), where the pulse energy is split into 4 sub-pulses. The experiments were performed with a pair of lenses f_1=+200mm and f_2=+10mm (Asphericon), which implies a demagnification ratio of M=20. Two axicons were used with base angle 1° and 2° (Asphericon), producing Bessel beams in the soda-lime glass at two different cone angles of θ_B of 6.7° and 13.3°. The core diameter decreases from 4.4 µm to 2.2 µm for the higher cone angle, while the theoretical length of the Bessel beam in the glass is l=860 µm for both cases. To preserve this length, the beam diameter was increased from 3.6 mm to 7.2 mm. The laser repetition rate of 10 kHz and the transverse sample translation velocity v=100 mm/s define a distance between subsequent bulk modifications of 10 µm. This distance is large enough to avoid the incubation effects which may affect the absorption of subsequent laser pulses [28]. Meanwhile, at a repetition rate of 10 kHz the next pulse arrives when the heat is dissipated, thus heat accumulation effects can be neglected [29].

The top view of the bulk modifications is recorded by optical transmission (OTM), cross-polarization (CPM), and phase contrast microscopy (PCM) as presented in Fig 1(b). For θ_B=6.7° in single pulse regime [Fig 1(b), top row], OTM reveals only weak modifications (photodarkening [30]). Corresponding CPM images show almost no stress associated with permanent modifications. On the other hand, using the same optical arrangement θ_B=6.7° in burst-mode regime, we observe strong and highly localized bulk modifications [Fig. 1(b), middle row]. These modifications appear as strong refractive index changes on PCM images, indicating local heating above the glass softening temperature [31]. Such permanent modifications lead to large surrounding residual stress as revealed under crossed polarizers. Furthermore, higher energy localization at larger conical angles, generates even stronger modifications. By keeping the energy of the burst constant and increasing the conical angle to θ_B=13.3° we are able to generate cracks [Fig. 1(b), bottom row].

Our results show that fs-bursts combined with spatial beam shaping provide an efficient tool for thermal and stress management, because the in-volume energy deposition can be controlled. Three interaction regimes can be defined leading to three distinctive type of modifications: i) weak modifications resulting mainly in point defects, ii) refractive index changes as a result of local heating and melting of the material, iii) highly efficient local heating with generation of cracks.

The third regime of modification leading to crack formation is of particular interest when it comes to cutting applications. In general, the crack orientation in transparent materials for linearly polarized beams with circular cross-section is not predefined, unless very short pulse durations are employed [11]. On the other hand, it is difficult to obtain ideal Bessel beams using commercially available refractive axicons, at least without performing additional spatial beam filtering [32]. Defects of fabrication will always lead to slightly elliptical profiles of the axicon near its tip, which can affect the propagation significantly. As shown in [33] for non-perfect axicons and machining with sub-ns pulses, a transversally distorted Bessel beam profile will lead to crack generation in a specific direction. In the case of fs-bursts, we also report large sensitivity towards the incident Bessel beam profile. Using our 52 µJ burst and Bessel beams with θ_B=13.3°, we have produced volume modifications in pristine glass in form of cracks. All cracks are generated in a certain, reproducible orientation. Simple rotation of the axicon by 90° produces cracks in orthogonal orientation, confirming that the non-ideal axicon is responsible for the transversal beam profile shaping. Thus, we have used this property of the axicon to control the crack direction for cutting along a straight line. Hereafter, the axicon was set such that the cracks are generated along the trajectory of sample translation, which results in an optimized edge quality due to absence of transversal cracks and easy pieces separation.

Optics EXPRESS

3. Numerical simulation of energy deposition

In order to understand the observed phenomena, we apply a multi-scale model covering the key physical processes eventually leading to permanent modifications of the glass through local heating. This model was previously developed to investigate the energy deposition of Gaussian femtosecond pulse trains focused with an objective [34], and is based on separation of the different time-scales involved, that is, fs–ps for pulse propagation and energy deposition, and µs for the thermal processes. Concerning the fs laser pulse propagation, we resort to an extended nonlinear optical Schrödinger equation accounting for self-focusing due to the optical Kerr effect and light defocusing via laser-generated conduction electrons [35]. For the considered case of linearly polarized light and moderate focusing conditions, the scalar and paraxial approximations are justified. Moreover, by comparing to a more complete unidirectional model [35, 36] it was checked that higher order effects like self-steepening can be neglected. Thus, the slowly varying complex optical field envelope $\mathcal{E}(r, \bar{t}, z)$ is governed by the following equation:

$$\begin{aligned}\partial_z \mathcal{E} =& \frac{i}{2k_0}\frac{1}{r}\partial_r r \partial_r \mathcal{E} - i\frac{k''}{2}\partial_{\bar{t}}^2 \mathcal{E} - \frac{\sigma}{2}N_e\mathcal{E} + i\frac{\omega_0 n_2}{c}I\mathcal{E} \\ & - i\frac{k_0}{2n_0^2 N_c}N_e\mathcal{E} - \frac{E_g W_{PI}(N_{nt}-N_e)}{2I}\mathcal{E}\end{aligned} \tag{1}$$

where n_0 and n_2 are the linear and nonlinear refractive indexes, respectively, k'' corresponds to the second order group velocity dispersion in the material, N_c is the critical electron density in the conduction band, E_g is the band gap, and $I(r, \bar{t}, z)$ is the laser pulse intensity, where the optical field envelope is normalized such that $I = |\mathcal{E}|^2$. The time $\bar{t}$ is the retarded time in a frame moving with the group velocity of the pulse at center frequency ω_0 and wave number $k_0 = n_0\omega_0/c$. The laser energy absorption by conduction band electrons is described by a Drude model with the cross section $\sigma = k_0 e^2\tau_c/[n_0^2\omega_0\varepsilon_0 m_e(1+\omega_0^2\tau_c^2)]$, where τ_c is an effective electron collision time. The evolution of the electron density in the conduction band $N_e(r, \bar{t}, z)$ reads

$$\partial_{\bar{t}} N_e = W_{\mathrm{PI}}(N_{nt} - N_e) + N_e\frac{\sigma I}{E_g} - \frac{N_e}{\tau_{\mathrm{rec}}} \tag{2}$$

where N_{nt} is the initial density of valence electrons, W_{PI} is the photo-ionization rate derived from Keldysh formula [37], and τ_{rec} is a recombination time for dielectric materials. As input condition for the laser pulses we employ axicon-generated Bessel beams. At the input surface of the glass sample ($z = 0$), we prescribe a Gaussian pulsed beam with a linear radial phase ramp corresponding to the cone angle

$$\mathcal{E}(z=0) = \mathcal{E}_0 \exp\left(-r^2/w_0^2 - ik_0 r\sin\theta_B\right)\exp\left(-\bar{t}^2/\tau_0^2\right) \tag{3}$$

For the cone angles θ_B of 13.3° and 6.7° we took initial beam widths w_0 of 180 µm and 90 µm, respectively, corresponding to the experiments. Moreover, note that the cone angles are defined inside the glass sample. Solving Eqs. (1) and (2) gives the spatial distribution of laser energy density $U(r, z)$ absorbed by the material. This deposited energy density is assumed to be fully transferred to the lattice few picoseconds after the interaction with a single sub-pulse, that is, much faster than the characteristic heat diffusion time.

The resulting energy density map is then used as a source term in a heat equation to compute the evolution of the thermal distribution. The model is evaluated for single pulses as well as for pulse trains composing a fs-burst to investigate the heat accumulation regime. Note that here the heat diffusion timescale is significantly longer than the total burst duration. Under the present conditions heat diffusion takes place on the order of μs (considering thermal diffusivity of D=0.6 mm^2/s and characteristic heat source transverse dimensions w of 1–2 µm, the cooling

Optics EXPRESS

time can be estimated as w^2/D). Therefore, the spatial profile of the lattice temperature increase is proportional to the energy deposition map $U(r, z)$. After each sub-pulse in the burst, the temperature increase ΔT can be obtained via the relation $\Delta T(r, z) = U(r, z)/\rho C$, where C is the specific heat capacity and ρ is the material density. All relevant material parameters used in the upcoming simulations are summarized in Table 1.

Table 1. Material parameters used to simulate femtosecond burst interaction with soda-lime glass [25, 34]

n_0	1.5134	σ [cm^2]	1.05×10^{-17}
n_2 [cm^2/W]	3.86×10^{-16}	τ_c [fs]	1.83
E_g [eV]	3.9	τ_{rec} [fs]	150
k'' [fs^2/cm]	286	ρ [g/cm^3]	2.44
N_c [cm^{-3}]	1.05×10^{21}	D [mm^2/s]	0.597
N_{nt} [cm^{-3}]	2.1×10^{22}	C [J/g K]	0.72

3.1. Energy deposition

Results of modeling the energy deposition in soda-lime glass with the numerical multi-scale model described above are illustrated in Fig. 2. First, we present the propagation of a 13 μJ Bessel pulsed beam in soda-lime glass at a conical angle of θ_B=6.7°. Such pulse energy is close to the energy contained in one sub-pulse of our fs burst. Following our experimental results presented in the previous section, we will consider three distinctive cases: propagation of single a 52 μJ pulse at θ_B=6.7°, and cumulative action of 4x13 μJ pulses propagating at θ_B=6.7° and 13.3°.

The linear propagation of a sinlge 13 μJ and 450 fs Bessel pulsed beam at conical interference angle θ_B=6.7° is illustrated in Fig 2(a). In this case, the fluence at zero interference order reaches 18 J/cm^2, which is significantly higher than the modification threshold of ≃3 J/cm^2 for single pulse surface ablation. Therefore, it can be anticipated that the electron conduction band will be populated and highly nonlinear effects will take place. Indeed, if we consider the full fs pulse propagation model as explained above, we observe a significant distortion of the fluence profile compared to the linear propagation case, as shown in Fig. 2(b). The central channel becomes larger with the fluence clamped at the level of 0.6 J/cm^2 corresponding to an intensity of 2.2 TW/cm^2. These values are typical for filamentary propagation [13]. The pulse energy is therefore deposited in this larger area with a diameter of 15 μm [Fig. 2(c)]. Despite the energy delocalization the central lobe, where we expect to find material modifications, is still well defined. Here, the concentration of free electrons reaches its maximum of N_e=10^{20} cm^{-3} and the deposited energy density is 290 J/cm^3. Increasing the pulse energy [Fig. 2(d)] does not lead to a higher deposited energy density, but only to an increase of the diameter of the laser absorption zone. For a 52 μJ pulse, the zone of energy deposition becomes more than 30 μm wide. On the other hand, a narrower Bessel beam constituted at θ_B=13.3° induces a higher intensity in the central channel up to 2.7 TW/cm^2. Consequently, a higher concentration of free electrons N_e=5×10^{20} cm^{-3} is produced and the deposited energy density reaches 905 J/cm^3 [see Fig. 2(e)]. The material modification is then localized in a channel with a much smaller diameter of 10 μm.

To further cross-check the model, we have measured the laser absorption using a power meter to get the time-averaged transmitted energy through the glass sample. The sample was translated in the plane perpendicular to the propagation axis at a sufficiently high speed to exclude incubation effects between two adjacent shots. After correcting the transmittance for the reflection at the glass/air interfaces, we have obtained a value of 49% for the nonlinear absorption of 13 μJ 450 fs pulses. Thus, our model overestimates the total absorption by predicting a value of 62%. Note that in our simulations, however, we employ perfect beam profiles, and interaction volumes may be therefore a bit larger than in the experiments. Due to imperfections of the axicon shape and in

Optics EXPRESS

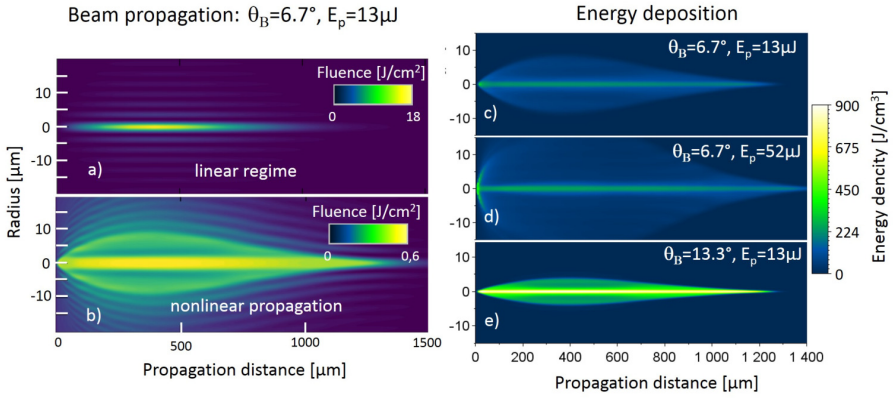

Fig. 2. Propagation of a Bessel beam produced by a 13 μJ 450 fs pulse at conical angle of θ_B=6.7°. a) The fluence distribution achieved in linear regime (all nonliearities set to zero) exceeds thresholds for self-focusing and photoionization by more than one order of magnitude. b) Fluence distribution in the nonlinear propagation regime. On the right, energy deposition maps obtained from fully nonlinear propagation for c) a single 13 μJ pulse at θ_B=6.7°, d) a single 52 μJ pulse at θ_B=6.7°, and a single 13 μJ pulse at θ_B=13.3°.

the experimental beam profile [32], a considerable amount of energy may propagate outside the interaction region.

For the modeling of the energy deposition by pulse trains, we have assumed that the optical properties of the material do not change much between two subsequent sub-pulses. Indeed, after time delay of 25 ns the free electrons are completely relaxed [38]. On the other hand, the presence of transient and permanent electron defects [28], as well as temperature increase inside the material [39] can induce a certain band collapse, and as a result, change the nonlinear absorption. We nevertheless neglect these effects because defects may be annealed by the next sub-pulses (a temperature increase of 200 K is sufficient [31]), and heating of more than 1000 K is required to reduce the bandgap sufficiently to enable multi-photon absorption of a lower order. As will be shown, our assumptions comply with the experimental parameters for the conical angle θ_B=6.7°. We suspect, however, that at higher conical angles, these effects alter the propagation dynamics to some extent and enhance the energy deposition.

Temperature maps obtained from our numerical modeling are illustrated in Figs. 3(a)–3(c). As expected, for the single 52 μJ pulse and θ_B=6.7°, the maximum temperature elevation is of the order of 150 K, which is not enough to reach the melting temperature and to induce permanent modifications. On the other hand, cumulative action of 4x13 μJ pulses in burst mode leads to a peak temperature of 750 K in the central part of the beam. The total duration of the laser matter interaction in burst mode (4 pulses) is 75 ns. At this time delay heat diffusion is not important, and temperature profiles follow the map of energy deposition for subsequent pulses. The peak temperature achieved during the interaction is close enough to the melting point of soda-lime glass, and refractive index changes and structural modifications are possible. Considering the cumulative action of a burst of 4x13 μJ pulses and θ_B=13.3°, as shown in Fig. 3(c), peak temperatures of 2150 K are achieved in a narrow region of 10 μm width. This temperature is far beyond the melting point, and strong temperature gradients may induce substantial thermal stress.

3.2. *Evaluation of thermal stress*

Based on the presented thermal maps, an estimation of both the induced stress and potential crack formation can be obtained. Our experimental observations have shown that the laser pulses

Optics EXPRESS

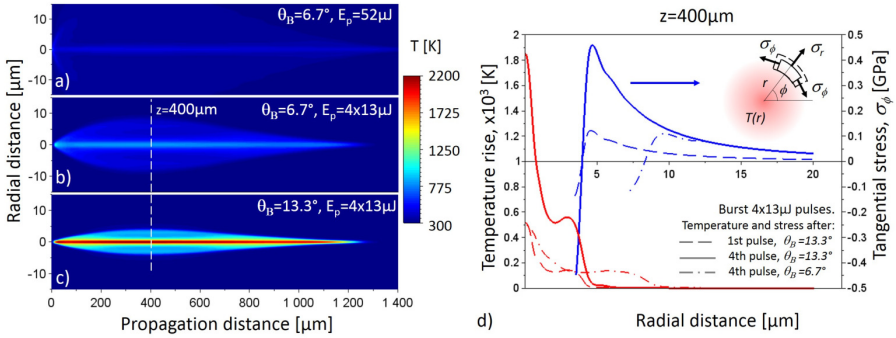

Fig. 3. Temperature maps after interaction with: a) a single 52 μJ pulse at θ_B=6.7°, b,c) cumulative action of a burst of 4x13 μJ pulses, propagating at b) θ_B=6.7° and c) θ_B=13.3°. Time delay between pulses in burst mode is 25 ns. Pulse duration of individual pulses is 450 fs. d) Temperature (red curves) and stress profiles (blue curves) produced in the xy plane at z=400 μm for 4x13 μJ bursts in different optical arrangements: after the first pulse for θ_B=13.3° (dashed line), after the fourth pulse at 75 ns for θ_B=13.3° (solid line) and θ_B=6.7° (dash-dotted line). In the inset, a scheme illustrating the stress components caused by thermal dilatation is shown.

induce only moderate modifications of density, meaning only small deformations of the glass matrix. Under these conditions, any hydrodynamic expansion may be neglected. The induced stress may thus be attributed to thermal dilatation. It is known that in glasses tensile stress is responsible for failure [40]. For a cylindrical heat source $T(r)$, it is the tangential component of the thermal stress σ_ϕ [see inset of Fig 3(d)]. Following [41], the relevant component is given by

$$\sigma_\phi(r) = \frac{aE}{1-\nu}\left(\frac{1}{r^2}\int_0^r T(r')r'dr' - T(r)\right) \tag{4}$$

where E=70 GPa is the Young modulus, a=80×10^{-7} K^{-1} the thermal dilatation coefficient for the soda-lime glass, and ν=0.78 is the Poisson coefficient. Taking temperature profiles in the xy plane at z=400 μm, the stress distribution can be calculated. The results are presented in Fig. 3(d).

In all configurations, the stress is maximum at the periphery of the modification, where the glass is below the transition temperature. Therefore, elastic behavior of glass is expected, that justifies our assumptions. For the larger Bessel beam with θ_B=6.7°, a temperature increase of 450 K and subsequent stress of 110 MPa are found (dash-dotted line). Because a stress of at least ~1 GPa is required to induce cracks in pristine glass [42], we do not expect crack generation under these conditions. However, when glass cools down, the deformations may freeze and give rise to permanent stress as experimentally observed according to Fig. 1(b).

In the regime of crack generation (4x13 μJ, θ_B=13.3°), already after the first pulse of the burst a stress of the order of 120 MPa is formed (dashed blue line). After the fourth pulse stress goes up to 0.5 GPa (solid blue line). This is still less than 1 GPa, however, the process of crack initiation is probabilistic due to presence of precursor defects. It turns out that crack generation has a certain probability even under lower stresses. This probability may increase substantially when the action of preceding pulses in the burst creates structural flaws in the medium. Thus, a crack may be formed in a circle of radius ~5 μm, where the stress is maximum, as shown in Fig. 3(d). When the crack is formed, the tensile stress required for its further opening lowers significantly down to 100–200 MPa [40,42]. Therefore, we expect a radial growth of the crack with the next pulses of the burst, as it was experimentally observed in [9].

Optics EXPRESS

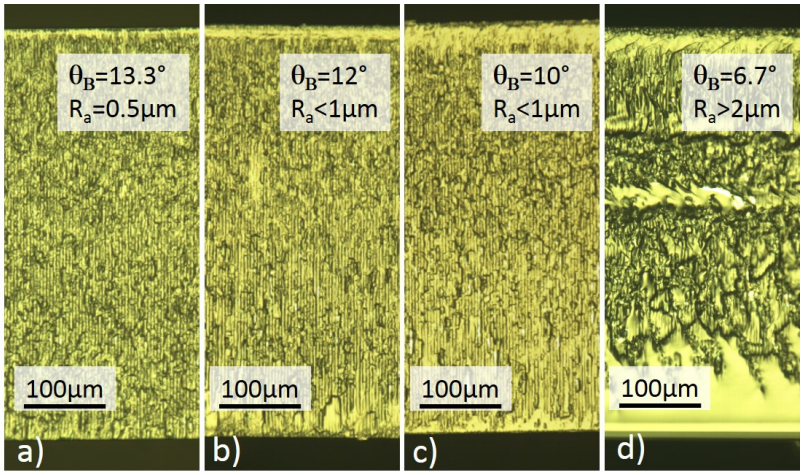

Fig. 4. Average roughness R_a of the sidewall after cutting of Eagle glass using internal scribing technique as a function of conical angle θ_B. The following experimental parameters were used: a) E_p=80 μJ, 4 sub-pulses, θ_B=13.3°, l=0.86 mm, b) E_p=98 μJ, 4 sub-pulses, θ_B=12°, l=1.05 mm, c) E_p=126 μJ, 4 sub-pulses, θ_B=10°, l=1.52 mm, d) E_p=74 μJ, 5 sub-pulses, θ_B=6.7°, l=0.86 mm. In all cases, the pulse repletion rate was 25 kHz, and the sample was translated at a speed of 100 mm/s.

4. Femtosecond bursts for glass cutting applications

4.1. *Internal volume scribing by using Bessel beam*

Strong material modifications associated with micro-cracks in the region of laser absorption considerably weakens the material locally. Therefore, by producing subsequent laser modifications along a certain trajectory with lateral distance of the order of a few μms, material weakening can be produced along a desired line, and pieces can be separated by applying some further mechanical cleaving. This is the principle of cutting by internal volume scribing [6]. Using this method, we cut a 500 μm thick Eagle glass in a single pass. Because of the low thermal expansion coefficient a=31.5×10^{-7} K^{-1} of this glass [26], absorbed pulses induce lower thermal stresses and micro-cracks are extended not further than 10 μm. Under these conditions, we observed that the weakening of this glass was more efficient when the separation between two adjacent irradiation spots was only 3–4 μm. At a repetition rate of 100 kHz and 80 μJ per pulse, cutting was possible at a speed 600 mm/s along a straight line.

Resulting average roughness of the sidewall largely depends on the size of the modification, which increases when the conical angle of interference of the Bessel beam is decreased as shown in Fig. 4. To vary the Bessel conical angle, an axicon with a base angle of 2° was used, while the demagnification was set to 20, 17.5 and 15 for the cases depicted in Figs. 4(a)–4(c), respectively. We observed the lowest roughness at θ_B=13.3°. When the conical angle was decreased, small chips occasionally rested at the front and bottom surfaces and the quality of the cuts was slightly reduced up to 1 μm roughness. At a conical angle of θ_B=6.7° (modifications were produced by the axicon with 1° base angle and demagnification of 20) it was hard to avoid nonlinear effects, even when splitting the pulse energy into 5 pulses per burst. It was difficult to maintain the high energy deposition along the sample thickness. In this case, as demonstrated in Fig. 4(d), glass separation revealed underexposed zones, where chipping occured, and the sidewall had a roughness >2 μm.

Optics EXPRESS

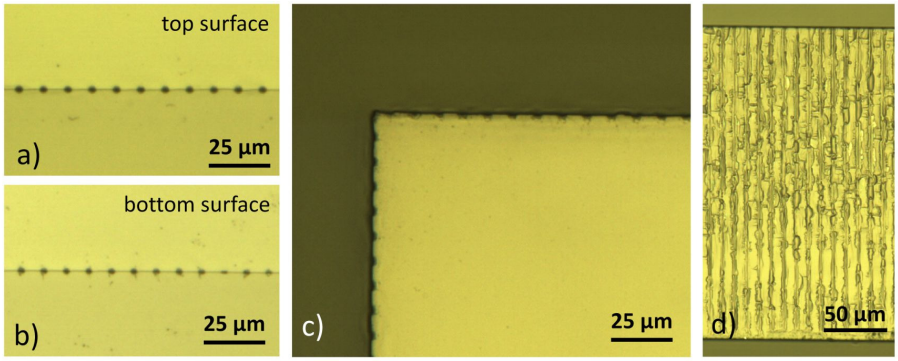

Fig. 5. Laser-induced cleaving of D263T glass by volume absorption of Bessel beams, E_p=70 µJ, 4 pulses per burst, θ_B=13.3°, 10 kHz, v=125 mm/s. a-b) microscopy images of laser entrance and exit surfaces, respectively. Black dots which result from initial laser modifications are joined by a thin crack on both surfaces. c) Top-view on the sample after cleaving reveals no chipping. d) Sidewalls have an average roughness R_a of less than 500 nm.

4.2. *Cleaving by laser-assisted controlled fracture propagation*

Another regime of cutting was produced in 250 µm thick D263T glass. This glass features a high thermal expansion a=80×10^{-7} K^{-1}, and thus rather extended cracks are generated upon laser irradiation. We have been using a Bessel beam of 600 µm length at θ_B=13.3° and a 70 µJ burst comprised of 4 pulses to produce cracks extending up to 20 µm. Translating the sample with a speed of 125 mm/s at pulse repletion rate of 10 kHz, a successive series of dots presenting a direct laser modification joined by a thin crack was achieved [Figs. 5(a) and 5(b)].

We are sure that we generated a through top/down crack, since it was detected on both surfaces of the sample corresponding to the laser entrance and exit. The presence of such through cracks means that the cut has been already performed by the laser and no additional mechanical force is needed for separation. Thus, we may speak of laser-assisted cleaving rather than a scribing technique, where sufficiently large mechanical forces are required to achieve separation. Larger spacing between subsequent modifications resulted in faster cleaving when working at the same laser repetition rate. This implies that cleaving by controlled fracture propagation is a more energy efficient process, which reduces unwanted modifications in the material. Proper alignment of the cracks with respect to the trajectory produces no chips and leads to a very low average roughness down to 200 nm for such thin glass as displayed in Figs. 5(c) and 5(d). We note that cutting of other hard and crystalline materials like sapphire, quartz, fused silica was equally achieved by using this technique.

5. Conclusion

We have investigated bulk processing of soda-lime and other silicate multicomponent glasses by means of fs laser pulses with spatial non-diffracting Bessel beam profiles. Our combined experimental and theoretical work demonstrates that the focusing geometry and the use of bursts of fs-pulses play a key role in depositing the laser energy in the glass with controllable efficiency. Three photo-inscription regimes have been identified in soda-lime glass, resulting in generation of defects, uniform refractive index modified structures, and micro-cracks. Numerical simulations supporting our experimental results show that when the energy of a single pulse is redistributed among sub-pulses in a burst, each sub-pulse undergoes less perturbations during the nonlinear propagation, and produces plasma in a more localized volume. Due to accumulation effects over the whole burst the total energy deposition on the optical axis is enhanced. We

Optics EXPRESS

demonstrated the practical relevance of our findings by producing oriented extended volume cracks for laser-assisted cleaving of glasses with various thickness.

Funding

French Ministry for the Economy and Finance (132906145, 132906146, 132906147); Grand Equipement National pour le Calcul Intensif (GENCI) (A0020510052); Qatar National Research Fund (QNRF) (NPRP 8-246-1-060).

Acknowledgments

We acknowledge the French Ministry for the Economy and Finance and the Aquitaine Regional Council for support and funding via the Femtoweld project. Numerical simulations were performed using computing resources at Mésocentre de Calcul Intensif Aquitain (MCIA) and GENCI. S.S. acknowledges support by the QNRF through the National Priorities Research Program (NPRP). We thank C. Javaux Léger for helping with the organization of the experiments.